International Journal of Solids and Structures 47 (2010) 1392–1404

Contents lists available at ScienceDirect

International Journal of Solids and Structures

journal homepage: www.elsevier.com/locate/ijsolstr

Implementation of the extended finite element method for dynamic thermoelastic fracture initiation

Arash Zamani [1], M. Reza Eslami [*,2]

Mechanical Engineering Department, Amirkabir University of Technology, P.O. Box 15875-4413, 424 Hafez Avenue, Tehran 15914, Iran

ARTICLE INFO

Article history:
Received 28 September 2009
Received in revised form 22 January 2010
Available online 2 February 2010

Keywords:
Thermoelasticity
Shock
XFEM
Fracture
SIF

ABSTRACT

The eXtended Finite Element Method (XFEM) is implemented to model the effect of the mechanical and thermal shocks on a body with a stationary crack. The classical thermoelasticity equations are considered. The Newmark and the Crank–Nicolson time integration schemes are used to solve the dynamical system of matrix equations obtained from the spatial discretization of the elastic and thermal parts respectively. The variation of dynamical stress intensity factors versus time are computed by the interaction integral method. A C++code is developed to do the different stages of the calculations from mesh generation to the calculation of interaction integrals. Several elastic and thermoelastic numerical examples are implemented, where the dynamical behaviour of the face and tip enrichments of XFEM are investigated and the results are discussed in detail.

1. Introduction

The Partition of Unity Method (PUM) (Melenk and Babuska, 1996) allows for the addition of a prior knowledge about the solution of a boundary value problem into the space of approximating functions. This is done through adding enrichment functions to the space of classical finite element approximations. The eXtended Finite Element Method (XFEM) (Belytschko and Black, 1999; Moës et al., 1999), initially considered for the fracture problems, uses a *local* partition of unity where a subset of nodes are enriched to allow strong or weak discontinuities to be modeled within an element. The nodes near to the crack tip can also be enriched with near tip asymptotic fields to reach required accuracy with coarser mesh resolutions. Discontinuity enrichment along the crack faces allows modeling of the arbitrary curved and growing cracks in a regular mesh. The asymptotic near tip enrichment leads to a considerable increase in the accuracy of computed SIFs. The XFEM is also successfully used in the other areas of the computational mechanics such as the fluid–structure interactions (Legay et al., 2006), phase transformations (Chessa et al., 2002), and biofilm growth (Duddu et al., 2008, 2009). The XFEM is also formulated to model the dislocations in continuum mechanics (Ventura et al., 2005; Gracie et al., 2007). Another interesting application is the combined space–time XFEM, which is developed to model the discontinuity propagation in dynamic problems (Chessa and Belytschko, 2004, 2006).

In the area of fracture mechanics, the XFEM is the subject of considerable research in the last decade. As some few examples, the following references may be addressed; (Sukumar et al., 2000; Moës et al., 2002; Gravouil et al., 2002) for modeling the three-dimensional cracks, (Daux et al., 2000) for arbitrary branched and intersecting cracks, (Moës and Belytschko, 2002; Zi and Belytschko, 2003) for cohesive crack growth, (Sukumar et al., 2003a) for bi-material interface crack, (Fries, 2008; Ventura et al., 2009) for considering the blending and integration issues in XFEM, (Bordas and Duflot, 2007; Duflot and Bordas, 2008) for error estimation and recovery, (Dumstorff and Meschke, 2007) for using different crack propagation criteria in predicting the crack growth path by XFEM, (Belytschko et al., 2003; Réthoré et al., 2005; Song and Belytschko, 2009) for treating dynamic issues, (Elguedj et al., 2007) for elastic–plastic fatigue crack growth, (Huynh and Belytschko, 2009) for fracture in composite materials and (Sukumar et al., 2003b) for fracture in polycrystalline microstructures. Also a nice description of an object-oriented programming for XFEM is given by Bordas et al. (2007).

The static case of thermoelastic fracture by XFEM is investigated in detail in (Duflot, 2008), where both 2*D* and 3*D* problems with different crack face thermal boundary conditions are included. In the present study, XFEM formulation is implemented in dynamic thermoelastic fracture initiation. The crack is assumed to be stationary and the fracture initiation under impact thermo-mechanical loading is considered. There are a number of elaborated works which have considered both fracture initiation and crack propagation under dynamic mechanical loading (Belytschko et al., 2003;

* Corresponding author. Tel.: +98 21 6454 3416; fax: +98 21 6641 9736.
E-mail address: eslami@aut.ac.ir (M.R. Eslami).
[1] Ph.D. student.
[2] Professor and Fellow of the Academy of Sciences.

0020-7683/$ - see front matter © 2010 Elsevier Ltd. All rights reserved.
doi:10.1016/j.ijsolstr.2010.01.024

Réthoré et al., 2005). A modified version is also proposed in (Song and Belytschko, 2009) to handle the complicated branching patterns and fragmentation.

The problem of thermoelastic fracture is also well studied by the numerical methods other than XFEM. As some few examples we may refer to (Wilson and Yu, 1979; Shih et al., 1986) for the use of J integral in the classical FEM modeling of thermal problems, (Zamani and Eslami, 2009) for the coupled thermoelasticity of a functionally graded cracked layer by the classical FEM, (Raveendra and Banerjee, 1992; Prasad et al., 1994) for using the boundary element method for thermal fracture problems, (Prasad et al., 1996; Dell'Erba et al., 1998) for the transient and 3D thermoelastic fracture with boundary element method, and (Hosseini-Tehrani et al., 2001, 2006) for using the coupled and generalized theories of thermoelasticity in thermal fracture by boundary element method.

In this study, the eXtended Finite Element Method (XFEM) is implemented to model the effect of the mechanical and thermal shocks on a cracked body. The robustness of the method for dynamic conditions is studied. The effect of crack tip position with respect to the elements edges and also the effect of adding singularity enrichment, are investigated in detail for *dynamic* loading of a *stationary* crack. Also the transient thermal conditions are mixed with both static and dynamic mechanical conditions and several discussions and interpretations are given about the results to explore the XFEM more in this area.

The present paper is organized as follows. In Section 2, the formulation of dynamic thermoelasticity for a cracked body by XFEM is given. The elements of mass, damping, and stiffness matrices obtained from XFEM discretization are presented in a simple form directly applicable in a computer code. In Section 3, the numerical integration is discussed and the treatment for each type of elements is clearly addressed. In Section 3, the domain form of interaction integral for dynamic thermoelasticity and extraction of SIFs is briefly described. Section 4 shows and discusses the dynamic behaviour of enrichment scheme by several thermo-mechanical numerical examples. Finally, Section 5 provides summary and concluding remarks.

2. Problem formulation

An isotropic homogeneous continuum Ω bounded by the boundary Γ is considered. The equations of motion and the first law of thermodynamics in the classical uncoupled form are

$$\frac{\partial \sigma_{ji}}{\partial x_j} + X_i = \rho \frac{\partial^2 u_i}{\partial t^2} \tag{1}$$

$$\frac{\partial q_i}{\partial x_i} + \rho c \frac{\partial T}{\partial t} = R \tag{2}$$

respectively. The stress tensor is related to the strain tensor by Hooke's law and the heat flux is related to temperature gradient by Fourier's law. These are

$$\sigma_{ij} = 2\mu\epsilon_{ij} + [\lambda\epsilon_{kk} - \alpha(3\lambda + 2\mu)(T - T_0)]\delta_{ij} \tag{3}$$

$$q_i = -k\frac{\partial T}{\partial x_i} \tag{4}$$

In these equations, u_i are the components of the displacement vector, σ_{ij} are the components of the stress tensor, ϵ_{ij} are the components of the strain tensor, T is the temperature, q_i are the components of the heat flux vector, ρ is the density, c is the specific heat, λ and μ are Lamé's constants, α is the thermal expansion coefficient, k is the thermal conductivity, X_i are the components of the body force vector, and R is the heat source. The associated boundary conditions are

$$T = \bar{T} \quad \text{on} \quad \Gamma_T, \quad q_i n_i = \bar{q} \quad \text{on} \quad \Gamma_q,$$
$$u_i = \bar{u}_i \quad \text{on} \quad \Gamma_u, \quad \sigma_{ji} n_j = \bar{t}_i \quad \text{on} \quad \Gamma_t \tag{5}$$

A crack Γ_c is assumed in Ω. The crack faces are assumed to be adiabatic and traction free. The space of admissible displacement and temperature fields are defined by

$$U = \{\mathbf{u} \in H_1^3(\Omega) : \mathbf{u} = \bar{\mathbf{u}} \quad \text{on} \quad \Gamma_u \quad \text{and} \quad \mathbf{u} \text{ discontinuous on } \Gamma_c\} \tag{6}$$

$$\Upsilon = \{T \in H_1(\Omega) : T = \bar{T} \quad \text{on} \quad \Gamma_T \quad \text{and} \quad T \text{ discontinuous on } \Gamma_c\} \tag{7}$$

The weak form can be expressed as: Find $\mathbf{u} \in U$ and $T \in \Upsilon$ such that

$$\int_\Omega \rho \delta u_i \frac{\partial^2 u_i}{\partial t^2}\, d\Omega + \int_\Omega \left[2\mu\epsilon_{ij}(\delta\mathbf{u})\epsilon_{ij}(\mathbf{u}) + \lambda\epsilon_{ll}(\delta\mathbf{u})\epsilon_{kk}(\mathbf{u})\right] d\Omega = \int_\Omega \delta u_i X_i\, d\Omega + \int_{\Gamma_t} \delta u_i \bar{t}_i\, d\Gamma + \int_\Omega \epsilon_{ll}(\delta\mathbf{u})\beta(T - T_0)\, d\Omega \tag{8}$$

$$\int_\Omega \rho c \delta T \frac{\partial T}{\partial t}\, d\Omega - \int_\Omega \frac{1}{k} q_i(\delta T) q_i(T)\, d\Omega = \int_\Omega \delta T R\, d\Omega - \int_{\Gamma_q} \delta T \bar{q}\, d\Gamma \tag{9}$$

where $(\delta\mathbf{u}, \delta T) \in U_0 \times \Upsilon_0$, and the subscript 0 denotes homogeneous essential conditions.

In the XFEM formulation, a standard local displacement approximation around the crack is enriched with discontinuous jump function across the crack faces and the asymptotic crack tip displacement field around the crack tip (Belytschko and Black, 1999; Moës et al., 1999) (Fig. 1). The same procedure is used for the temperature enrichment (Duflot, 2008). The formulation of the XFEM for displacement components can be written as

$$\mathbf{u}(x,y) = \sum_{n\epsilon N} N_n(x,y)\mathbf{a}_n + \sum_{n\epsilon N_{cr}} N_n(x,y)[H(x,y) - H(x_n,y_n)]\mathbf{b}_n + \sum_{n\epsilon N_{tip}} N_n(x,y) \sum_{m=1}^{M} [F_m(r,\theta) - F_m(r_n,\theta_n)]\mathbf{c}_{nm} \tag{10}$$

where N_{cr} is the set of nodes whose support is crossed by the crack faces, while N_{tip} is the set of nodes inside a predefined area around the crack tip. Here, $\{F_m\}$ is a basis that spans the singular term of near tip asymptotic fields

$$\{F_m\} = \left\{\sqrt{r}\, \sin\frac{\theta}{2},\ \sqrt{r}\, \cos\frac{\theta}{2},\ \sqrt{r}\, \sin\frac{\theta}{2}\, \cos\theta,\ \sqrt{r}\, \cos\frac{\theta}{2}\, \cos\theta\right\} \tag{11}$$

where r and θ are the usual crack-tip polar coordinates. In this study the crack faces are assumed to be adiabatic so the temperature is discontinuous along the crack faces and the heat flux is singular at the crack tip (Sih, 1962). The leading term of the asymptotic field for temperature of an adiabatic crack can be written as (Duflot, 2008)

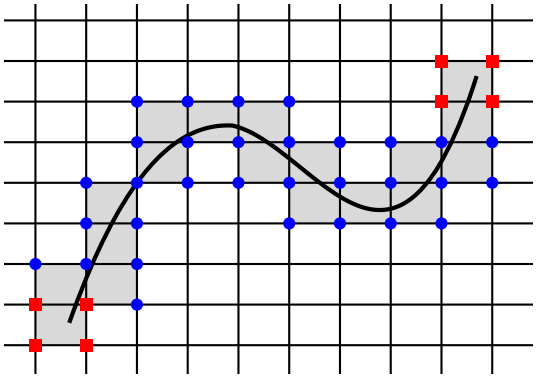

Fig. 1. Selection of enriched nodes for 2D crack problem. Circled nodes (set of nodes N_{cr}) are enriched by the discontinuity function whereas the squared nodes (set of nodes N_{tip}) are enriched by the crack tip functions. The gray elements are those cut by the crack.

$$T = -\frac{K_T}{k}\sqrt{\frac{2r}{\pi}}sin\left(\frac{\theta}{2}\right) \tag{12}$$

Thus, the temperature field is discretized similar to the displacement field, but with only the first branch function (11), which is the only discontinuous branch function

$$T(x,y) = \sum_{n\epsilon N} N_n(x,y)a_n + \sum_{n\epsilon N_{cr}} N_n(x,y)[H(x,y) - H(x_n,y_n)]b_n + \sum_{n\epsilon N_{tip}} N_n(x,y)[F_1(r,\theta) - F_1(r_n,\theta_n)]c_n \tag{13}$$

Eqs. (10) and (13) are substitute into the weak form of the governing equations, Eqs. (1) and (2), and the element matrices are obtained by standard Bubnov–Galerkin procedures. Eqs. (10) and (13) can be written in the following compact form

$$\mathbf{u}(x,y) = \sum_{n\epsilon N} N_n(x,y)\mathbf{a}_n + \sum_{n\epsilon N_{en}} \Phi_n(x,y)\mathbf{b}_n \tag{14}$$

$$T(x,y) = \sum_{n\epsilon N} N_n(x,y)a_n + \sum_{n\epsilon N_{en}} \Psi_n(x,y)b_n \tag{15}$$

where $\Phi_n(x,y)$ and $\Psi_n(x,y)$ stand for the enriched parts of the displacement and temperature fields, respectively. They can be related to either face or tip enrichment. Based on this compact notation, we now drive the element matrices of the thermal and elastic parts of the problem. First, the thermal part of the problem and then the elastic part are considered. The vector of unknowns for temperature is assumed in the form $Unknowns = \{a_i, b_i\}^T$. In this notation the damping matrix, stiffness matrix, and the force vector of thermal part of the problem are

$$[C^{Thermal}] = \begin{bmatrix} [C^{aa}] & [C^{ab}] \\ Sym. & [C^{bb}] \end{bmatrix} \tag{16}$$

$$[K^{Thermal}] = \begin{bmatrix} [K^{aa}] & [K^{ab}] \\ Sym. & [K^{bb}] \end{bmatrix} \tag{17}$$

$$\{F^{Thermal}\}^T = \{\{F^a\}^T \quad \{F^b\}^T\} \tag{18}$$

where

$$[C^{aa}] = \int_\Omega \rho c N_i N_j \, d\Omega \quad [C^{ab}] = \int_\Omega \rho c N_i \Psi_j \, d\Omega$$

$$[C^{bb}] = \int_\Omega \rho c \Psi_i \Psi_j \, d\Omega$$

$$[K^{aa}] = \int_\Omega k\left\{\frac{\partial N_i}{\partial x}\frac{\partial N_j}{\partial x} + \frac{\partial N_i}{\partial y}\frac{\partial N_j}{\partial y}\right\} d\Omega$$

$$[K^{ab}] = \int_\Omega k\left\{\frac{\partial N_i}{\partial x}\frac{\partial \Psi_j}{\partial x} + \frac{\partial N_i}{\partial y}\frac{\partial \Psi_j}{\partial y}\right\} d\Omega$$

$$[K^{bb}] = \int_\Omega k\left\{\frac{\partial \Psi_i}{\partial x}\frac{\partial \Psi_j}{\partial x} + \frac{\partial \Psi_i}{\partial y}\frac{\partial \Psi_j}{\partial y}\right\} d\Omega$$

$$\{F^a\} = \int_\Omega N_i R \, d\Omega - \int_{\Gamma_q} N_i \bar{q} \, d\Gamma \quad \{F^b\} = \int_\Omega \Psi_i R \, d\Omega - \int_{\Gamma_q} \Psi_i \bar{q} \, d\Gamma$$

We now turn to the elastic part. The vector of unknowns for displacement is assumed in the form $Unknowns = \{a_i^u, a_i^v, b_i^u, b_i^v\}^T$. The superscripts u and v refer to x and y components of displacement, respectively. In this notation the mass matrix, stiffness matrix, and the force vector of elastic part of the problem are

$$[M^{Elastic}] = \begin{bmatrix} [M^{aa}] & [0] & [M^{ab}] & [0] \\ & [M^{aa}] & [0] & [M^{ab}] \\ & & [M^{bb}] & [0] \\ & Sym. & & [M^{bb}] \end{bmatrix} \tag{19}$$

$$[K^{Elastic}] = \begin{bmatrix} [K_{uu}^{aa}] & [K_{uv}^{aa}] & [K_{uu}^{ab}] & [K_{uv}^{ab}] \\ & [K_{vv}^{aa}] & [K_{vu}^{ab}] & [K_{vv}^{ab}] \\ & & [K_{uu}^{bb}] & [K_{uv}^{bb}] \\ & Sym. & & [K_{vv}^{bb}] \end{bmatrix} \tag{20}$$

$$\{F^{Elastic}\}^T = \{\{F_u^a\}^T \ \{F_v^a\}^T \ \{F_u^b\}^T \ \{F_v^b\}^T\} \tag{21}$$

where

$$[M^{aa}] = \int_\Omega \rho N_i N_j \, d\Omega \quad [M^{ab}] = \int_\Omega \rho N_i \Phi_j \, d\Omega \quad [M^{bb}] = \int_\Omega \rho \Phi_i \Phi_j \, d\Omega$$

$$[K_{uu}^{aa}] = \int_\Omega \left\{(2\mu+\lambda)\frac{\partial N_i}{\partial x}\frac{\partial N_j}{\partial x} + \mu\frac{\partial N_i}{\partial y}\frac{\partial N_j}{\partial y}\right\} d\Omega$$

$$[K_{uv}^{aa}] = \int_\Omega \left\{\mu\frac{\partial N_i}{\partial y}\frac{\partial N_j}{\partial x} + \lambda\frac{\partial N_i}{\partial x}\frac{\partial N_j}{\partial y}\right\} d\Omega$$

$$[K_{vv}^{aa}] = \int_\Omega \left\{\mu\frac{\partial N_i}{\partial x}\frac{\partial N_j}{\partial x} + (2\mu+\lambda)\frac{\partial N_i}{\partial y}\frac{\partial N_j}{\partial y}\right\} d\Omega$$

$$[K_{uu}^{ab}] = \int_\Omega \left\{(2\mu+\lambda)\frac{\partial N_i}{\partial x}\frac{\partial \Phi_j}{\partial x} + \mu\frac{\partial N_i}{\partial y}\frac{\partial \Phi_j}{\partial y}\right\} d\Omega$$

$$[K_{uv}^{ab}] = \int_\Omega \left\{\mu\frac{\partial N_i}{\partial y}\frac{\partial \Phi_j}{\partial x} + \lambda\frac{\partial N_i}{\partial x}\frac{\partial \Phi_j}{\partial y}\right\} d\Omega$$

$$[K_{vu}^{ab}] = \int_\Omega \left\{\mu\frac{\partial N_i}{\partial x}\frac{\partial \Phi_j}{\partial y} + \lambda\frac{\partial N_i}{\partial y}\frac{\partial \Phi_j}{\partial x}\right\} d\Omega$$

$$[K_{vv}^{ab}] = \int_\Omega \left\{\mu\frac{\partial N_i}{\partial x}\frac{\partial \Phi_j}{\partial x} + (2\mu+\lambda)\frac{\partial N_i}{\partial y}\frac{\partial \Phi_j}{\partial y}\right\} d\Omega$$

$$[K_{uu}^{bb}] = \int_\Omega \left\{(2\mu+\lambda)\frac{\partial \Phi_i}{\partial x}\frac{\partial \Phi_j}{\partial x} + \mu\frac{\partial \Phi_i}{\partial y}\frac{\partial \Phi_j}{\partial y}\right\} d\Omega$$

$$[K_{uv}^{bb}] = \int_\Omega \left\{\mu\frac{\partial \Phi_i}{\partial y}\frac{\partial \Phi_j}{\partial x} + \lambda\frac{\partial \Phi_i}{\partial x}\frac{\partial \Phi_j}{\partial y}\right\} d\Omega$$

$$[K_{vv}^{bb}] = \int_\Omega \left\{\mu\frac{\partial \Phi_i}{\partial x}\frac{\partial \Phi_j}{\partial x} + (2\mu+\lambda)\frac{\partial \Phi_i}{\partial y}\frac{\partial \Phi_j}{\partial y}\right\} d\Omega$$

$$\{F_u^a\} = \int_\Omega N_i X_1 \, d\Omega + \int_{\Gamma_t} N_i \bar{t}_1 d\Gamma + \int_\Omega \frac{\partial N_i}{\partial x}\beta(T-T_0)\, d\Omega$$

$$\{F_v^a\} = \int_\Omega N_i X_2 \, d\Omega + \int_{\Gamma_t} N_i \bar{t}_2 \, d\Gamma + \int_\Omega \frac{\partial N_i}{\partial y}\beta(T-T_0)\, d\Omega$$

$$\{F_u^b\} = \int_\Omega \Phi_i X_1 \, d\Omega + \int_{\Gamma_t} \Phi_i \bar{t}_1 \, d\Gamma + \int_\Omega \frac{\partial \Phi_i}{\partial x}\beta(T-T_0)\, d\Omega$$

$$\{F_v^b\} = \int_\Omega \Phi_i X_2 \, d\Omega + \int_{\Gamma_t} \Phi_i \bar{t}_2 \, d\Gamma + \int_\Omega \frac{\partial \Phi_i}{\partial y}\beta(T-T_0)\, d\Omega$$

The formulations presented for the element matrices and force vectors are used in the computer code in four steps:

1. The classical part of finite element is computed for all elements.
2. The tip enrichment is computed for related elements.
3. The face enrichment is computed for related elements.
4. The interaction between tip and face enrichments is computed for elements containing both types of enrichments. In this case, the nomenclature in the vector of unknowns and the formulations presented above should be changed accordingly.

After the system matrices are constructed, the Crank–Nicolson scheme (trapezoidal rule) and the Newmark integration algorithm are used to obtain the dynamical response for the thermal and elastic parts respectively.

Following (Eslami, 2003), for time integration of the transient heat conduction problem, the unknown vector $\{X\}$ at time $t + \Delta t$ is approximated as

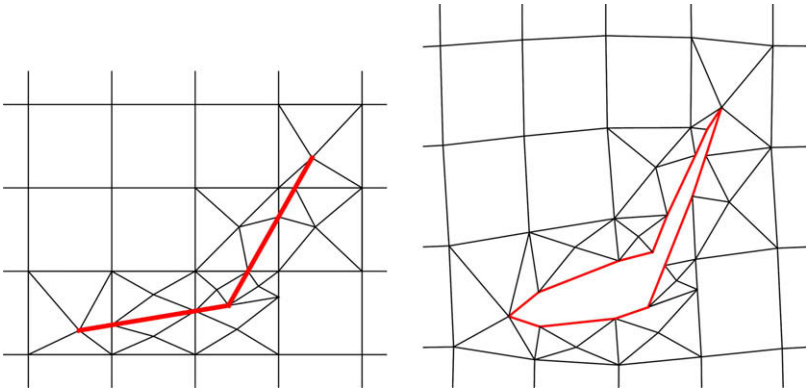

Fig. 2. Sub-triangles used for numerical integration. Left: undeformed. Right: deformed under vertical tension.

$$\{X\}_{t+\Delta t} = \{X\}_t + \left[(1-\beta)\{\dot{X}\}_t + \beta\{\dot{X}\}_{t+\Delta t}\right](\Delta t), \tag{22}$$

where different values of the parameter β are associated with various numerical schemes. For $\beta = \frac{1}{2}$ the Crank–Nicolson scheme (trapezoidal rule) is obtained which is unconditionally stable and do *not* introduce numeric dissipation into the solution results.

For the elastic part of the problem the Newmark method is used (Newmark, 1959). Following (Eslami, 2003), the unknown vector $\{X\}$ and its derivative $\{\dot{X}\}$ at time $t + \Delta t$ are approximated in terms of their values at time t as

$$\{\dot{X}\}_{t+\Delta t} = \{\dot{X}\}_t + [(1-\alpha)\{\ddot{X}\}_t + \alpha\{\ddot{X}\}_{t+\Delta t}]\Delta t \tag{23}$$
$$\{X\}_{t+\Delta t} = \{X\}_t + \{\dot{X}\}_t \Delta t + \left[\left(\frac{1}{2}-\beta\right)\{\ddot{X}\}_t + \beta\{\ddot{X}\}_{t+\Delta t}\right](\Delta t)^2$$

where the coefficients α and β are parameters which determine the accuracy and stability of the numerical technique. For $\alpha \geqslant \frac{1}{2}$ and $\beta \geqslant \frac{\alpha}{2}$ the scheme is unconditionally stable. In this study, these two parameters are chosen to be $\alpha = \frac{1}{2}$ and $\beta = \frac{1}{4}$ (implicit mean acceleration scheme). For these values of these two parameters, the numeric dissipation due to the scheme is zero and the total energy $\frac{1}{2}(\{\dot{X}\}^T[M]\{\dot{X}\} + \{X\}^T[K]\{X\})$ remains constant in the absence of external forces (Hughes and Belytschko, 2000; Réthoré et al., 2004). Thus the stability and discretized energy balance are guaranteed by these values of α and β for our application which includes dynamic thermo-mechanical loading of a stationary crack. For the case of a dynamically growing crack, the stability and discretized energy balance need much more elaboration for both standard FEM (Réthoré et al., 2004) and XFEM (Réthoré et al., 2005).

A C++code is developed to do the different stages of the calculations from mesh generation to the calculation of interaction integrals. For solving the system of matrix equations, the conjugate gradient method from the efficient iterative solver package, IML++ (Dongarra et al., 1998) is used in combination with the nice sparse matrix class library, SparseLib++ (Pozo et al., 1998).

3. Numerical integration

The integration classification is done based on the type of the function being integrated and also the type of the element on which the integration is performed.

For the elements that are cut by the crack and have discontinuity enrichment, the standard Gauss quadrature is not adequate for numerical integration. These elements are divided into some sub-triangles with boundaries on the crack faces and element edges and then the Gauss quadrature formula is implemented for each of these sub-triangles (Moës et al., 1999). The free C++code available in Professor N. Sukumar's homepage (Sukumar, 2000), which generates sub-triangles for an element crossed by a straight line, is extended here for elements containing crack kink and also for polar configuration in elements containing crack tip. Fig. 2 shows the generated sub-triangles for a multiple segment crack. These sub-triangles are also used for computing the element area below and above the crack and to set a criteria for node enrichment with discontinuity function (Dolbow et al., 2000).

For integrands containing standard shape functions or face enrichment functions, a bidirectional Gauss quadrature with three order in each direction is used for the rectangular elements and a four order direct Gauss quadrature is used for the sub-triangles.

For the integrands containing tip enrichment functions, the corresponding element may have the crack tip inside or outside. For elements containing crack tip inside them, the element is divided into a set of sub-triangles with a polar configuration having one vertex in common with the crack tip (Fig. 3). In each sub-triangle a singular mapping is performed (Laborde et al., 2005) and a bidirectional Gauss quadrature with 15 order in each direction is used. Use of the singular mapping increases drastically the accuracy of integration of singular functions. In the absence of singular mapping, a very large number of Gauss quadrature points should be used in elements containing the crack tip. For elements not containing the crack tip but have tip enrichment, a bidirectional Gauss quadrature with 23 order in each direction is used for rectangular elements and a 12 order direct Gauss quadrature is used for sub-triangles. The high order used for these elements is because the crack tip may be too close to them while being still outside them. For the integrands containing combinations of tip and face enrichments a similar scheme is used.

At this point, let us to mention some recent efforts to facilitate the process of numerical integration in XFEM. In the work by Ventura (2006), the need for constructing sub-cells in numerical integration of discontinuity functions is removed by defining an equivalent polynomial function whose integral over the element

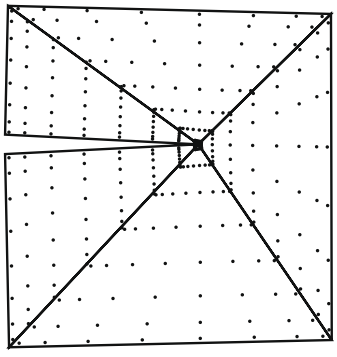

Fig. 3. Gauss quadrature points in the element containing the crack tip.

area is equal to the integral of discontinuity function. However that method needs still further developments to treat cases in which a quadrilateral element of an unstructured mesh is mapped onto a parent element and also in cases in which a crack kink exists inside an element. In another work by Ventura et al. (2009), a scheme was proposed to reduce the computational cost of evaluating integrands containing crack tip singular functions. In that work, the integration over the element area was replaced by a contour integral over the element boundary by divergence theorem. However, that method is applicable only to elements for which all nodes of the element are enriched and for which all enriched degrees of freedom at all nodes of the element are equal. In the work by Natarajan et al. (2009), the Schwarz–Christoffel conformal mapping was used to map an arbitrary polygon onto a unit disk on which the numerical integration is performed. Integrating over a polygonal is also studied by Mousavi et al. (2009). The group theory and numerical optimization were invoked in that work to compute appropriate quadrature rules over concave and convex polygons. The other scheme for the numerical integration is by the use of smoothed finite element method (Liu et al., 2006; Nguyen-Xuan et al., 2008; Nguyen et al., 2008a; Bordas et al., 2009). In this scheme, after dividing the element into sub-triangles, the integration is performed over the boundaries of the triangles.

4. Interaction integral and thermal dynamical stress intensity factors

The interaction integral is formulated by superimposing the actual and auxiliary fields on the path independent J-integral. The J integral can be written as the following integral over a vanishingly small contour surrounding the crack tip

$$J = \lim_{\Gamma_0 \to 0} \int_{\Gamma_0} \left[(W+K)\delta_{1i} - \sigma_{ij}\frac{\partial u_j}{\partial x_1} \right] n_i \, d\Gamma \tag{24}$$

where W and K are the strain energy and kinetic energy densities, respectively. The form of Eq. (24) is not suitable for numerical analysis since it is not feasible to evaluate the stresses and strains along a vanishingly small contour. A closed contour Γ^* is considered as in Fig. 4 ($\Gamma^* = \Gamma_1 + \Gamma_+ + \Gamma_- + \Gamma_0$). Eq. (24) is written along this contour with the help of a weighting function q that is unity on Γ_0 and zero on Γ_1

$$J = \int_{\Gamma^*} \left[\sigma_{ij}\frac{\partial u_j}{\partial x_1} - (W+K)\delta_{1i} \right] q m_i \, d\Gamma - \int_{\Gamma^+ + \Gamma^-} \sigma_{2j}\frac{\partial u_j}{\partial x_1} q \, d\Gamma \tag{25}$$

The crack faces are assumed to be traction free. Applying the divergence theorem and using the equilibrium and strain–displacement equations, after some manipulations, give

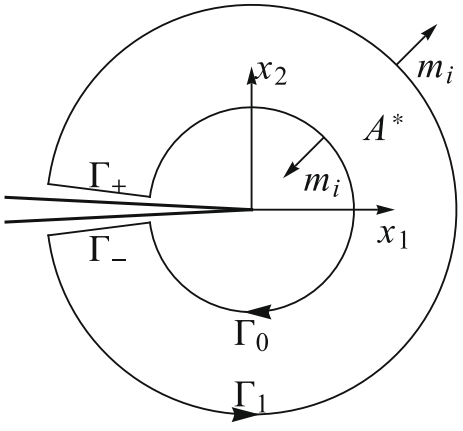

Fig. 4. J integral contour around the crack tip.

$$J = \int_{A^*} \left\{ \left[\sigma_{ij}\frac{\partial u_j}{\partial x_1} - (W+K)\delta_{1i} \right] \frac{\partial q}{\partial x_i} + \left[\rho \frac{\partial^2 u_j}{\partial t^2}\frac{\partial u_j}{\partial x_1} + \alpha\sigma_{kk}\frac{\partial T}{\partial x_1} - \rho\frac{\partial u_j}{\partial t}\frac{\partial^2 u_j}{\partial x_1 \partial t} \right] q \right\} dA \tag{26}$$

Two states of a cracked body are considered. State 1, corresponds to the present state and state 2, is an auxiliary state which will be chosen as the asymptotic fields for modes I or II. The J-integral for the sum of the two states can be written as

$$J^{(1+2)} = J^{(1)} + J^{(2)} + I^{(1,2)} \tag{27}$$

where $I^{(1,2)}$ is called the interaction integral between states 1 and 2. For general mixed-mode loading, the value of the J-integral is related to the stress intensity factors as

$$J = \frac{K_I^2}{E^*} + \frac{K_{II}^2}{E^*} E^* = \begin{cases} E & \text{plane stress} \\ E/(1-\nu^2) & \text{plane strain} \end{cases} \tag{28}$$

Using Eqs. (27) and (28), the relation between the interaction integral and stress intensity factors is obtained as

$$I^{(1,2)} = \frac{2}{E^*}(K_I^{(1)}K_I^{(2)} + K_{II}^{(1)}K_{II}^{(2)}) \tag{29}$$

Defining the state 2 as the pure mode I asymptotic field, gives the mode I stress intensity factor for the state 1 as

$$K_I^{(1)} = \frac{E^*}{2} I^{(1,\ model)} \tag{30}$$

In a similar way, mode II stress intensity factor can be obtained from the value of the interaction integral. From Eqs. (26) and (27), the interaction integral is obtained as

$$I^{(1,2)} = \int_{A^*} \left\{ \left[\sigma_{ij}^{(1)}\frac{\partial u_j^{(2)}}{\partial x_1} + \sigma_{ij}^{(2)}\frac{\partial u_j^{(1)}}{\partial x_1} - W^{(1,2)}\delta_{1i} \right] \frac{\partial q}{\partial x_i} + \left[\rho\frac{\partial^2 u_j^{(1)}}{\partial t^2}\frac{\partial u_j^{(2)}}{\partial x_1} + \alpha\sigma_{kk}^{(2)}\frac{\partial T^{(1)}}{\partial x_1} \right] q \right\} dA \tag{31}$$

where $W^{(1,2)}$ is the interaction strain energy density

$$W^{(1,2)} = \sigma_{ij}^{(1)}\epsilon_{ij}^{(2)} = \sigma_{ij}^{(2)}\epsilon_{ij}^{(1)} \tag{32}$$

The term ϵ_{ij} in (32) is the elastic part of the strain tensor. For thermoelastic plane strain conditions, the term ϵ_{33} of the elastic part of the strain tensor has nonzero value to have zero sum with thermal part.

5. Numerical examples

5.1. Internally cracked plate under mechanical shock

An elastic two-dimensional layer with an internal crack is considered, as is shown in Fig. 5. The layer is under tension stress shock on its upper and lower surfaces. The assumed boundary conditions result into a mode I crack opening problem. The SIF values for this two-dimensional elasticity problem are obtained and compared with the analytical solution given by Freund (1990). This analytical solution is used by (Duarte et al., 2001) to investigate the accuracy of their generalized finite element results. The plane strain condition is assumed. As in (Duarte et al., 2001), a uniform traction of magnitude $\sigma_0 = 63750.0$ Pa is applied at time $t = 0$ as a step function to the upper and lower surfaces. The layer dimensions are $h = 2.0$ m and $w = 10.0$ m and the crack length is $a = 5.0$ m. The analytical solution in (Freund, 1990) is for an infinite layer. Since the assumed layer is finite, the calculations are carried out to the point $t = 0.001$ s before the reflected wave from

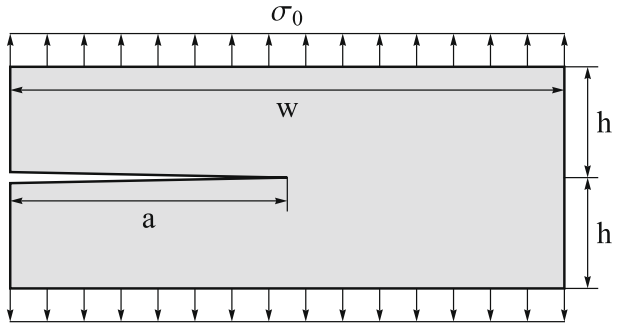

Fig. 5. First numerical example: internally cracked plate under mechanical shock.

the edge reaches the crack tip. The material properties are $\rho = 7833\ \mathrm{kg/m^3}$, $E = 200$ GPa and $\nu = 0.30$.

The percentage errors are also given in some figures in companion with the SIFs figures. The percentage error is defined as follow

$$\text{Percentage error } (t) = 100 \times \frac{K_I^{XFEM}(t) - K_I^{Analytical}(t)}{K_I^{Analytical}(t_2)} \tag{33}$$

where t_2 is equal to 0.001 s.

Three different cases are considered. In each of these cases, three different mesh resolutions are considered. For the first and second cases, the number of elements in each direction are 100×50, 200×100 and 400×200. For the third case the number of elements in each direction are 101×51, 201×101 and 401×201. For all three cases, the number of time steps are $N_{Time} = 150, 300$ and 600.

In the first and second cases, even number of elements in each direction are used such that the crack lies on the elements edges and the crack tip coincides with one of the nodes. In these conditions, it is possible to locate the exact position of the crack tip by using the discontinuity enrichment alone without using the singularity enrichment. The only effect is the reduction of the accuracy of the approximating space near the crack tip. Now, the effect of using singularity enrichment could be examined. In the first case only discontinuity enrichment is used (Fig. 6) and in the second case nine nodes around the crack tip are enriched with singular branch functions (Fig. 7). It could be seen from Figs. 6 and 7 that there is about several 0.1% difference for the mean value of the error (ignoring oscillations) between the two cases.

In the third case, the crack tip position with respect to the element edges is changed and the effects of singularity enrichment and discontinuity enrichment are compared with the ones in the two previous cases. In the third case, odd number of elements are used in each direction. So the crack tip is located at the element centroid (Fig. 8) in contrast to the cases one and two where the crack tip was coincident to one of the nodes. As can be seen from Figs. 7 and 8, the method shows an acceptable amount of robustness to the change of crack tip position with respect to the element edges. The noisy oscillations are larger for the case of crack tip locating at the centeroid of an element, but some of it may be due to the change of optimal number of time steps by changing the crack tip position.

From Figs. 6–8, it is observed that there are some noisy oscillations in the computed SIF values specially near time $t = 0.000341$ s where the wave front reaches the crack tip and SIF value begins to abruptly grow from zero. These unavoidable oscillations

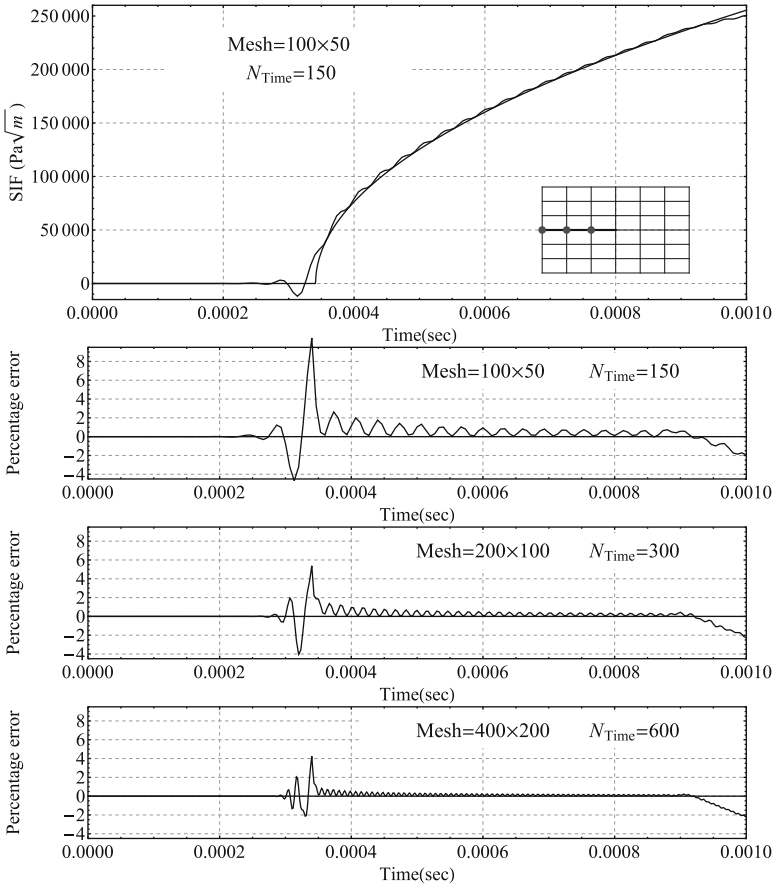

Fig. 6. Stress intensity factor versus time for the case 1 of the first numerical example.

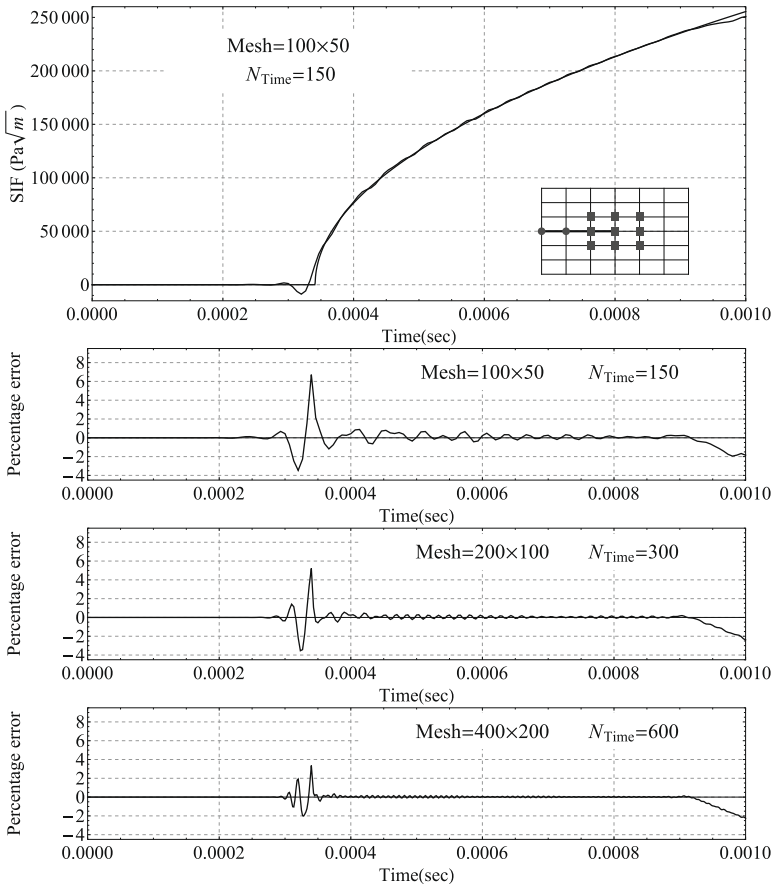

Fig. 7. Stress intensity factor versus time for the case 2 of the first numerical example.

are also observed in (Zamani and Eslami, 2009; Belytschko et al., 2003; Réthoré et al., 2005; Duarte et al., 2001) for the standard, extended, and generalized FEM. These oscillations are the characteristic of the solution of a shock propagation problem by the finite element discretization in the spatial domain and also by the Newmark method in the time domain, since these two both are considered originally for smooth behaviour of the solution. As could be seen from Figs. 6–8, increasing the mesh resolution and the number of time steps decreases these noisy oscillations.

It seems that it is possible to choose a suitable ratio between the mesh resolution in the direction of the wave motion and the number of time steps to minimize the noisy oscillations (as is done in this numerical example). But in general, they cannot be completely eliminated in the authors' knowledge. An effect of changing this ratio is to place the majority of oscillations before or after the moving shock front as could be seen by comparing Fig. 6 with Fig. 9.

The blending effect treated in detail in (Fries, 2008; Ventura et al., 2009) is an important issue in the extended finite element method. A magnifying factor for these noisy oscillations may be the blending effect. Increasing the number of nodes that are enriched by singularity functions would decrease the effect of blending. Also, a more systematic approach would be the use of weighting functions (Fries, 2008; Ventura et al., 2009).

For static problems, it is proposed by Laborde et al. (2005) to constraint the enriched DOFs at different nodes to have equal values (DOF gathering) for better conditioning of the system matrices and also for a reduction in total number of DOFs. This scheme would not be convenient for dynamic problems, since constraining several layers of nodes around crack tip leads to a miss of correct velocity for the shock motion in the region near to the crack tip.

At time $t = 0.001023$ s the reflected waves from finite boundaries reach the crack tip and invalidate the assumption of infinite boundary for which the analytical SIFs are available. But as can be seen from Figs. 6–8, for all three cases the numerical SIF begins to depart the analytical SIF at some time before the predicted one. The reason is not clear to the authors. In (Réthoré et al., 2005) this behaviour is also observed and the reason is said to be the arrival of the reflected wave to the domain of interaction integral. It can be argued that this could not be the reason because there is a same amount of departure for different sizes of interaction integral domains.

5.2. Edge cracked plate under quasi static thermal shock

An elastic two-dimensional layer with an edge crack is considered, as is shown in Fig. 10. The layer is rapidly cooled by conduction at its left surface to T_e which is assumed to be equal to -10 K in this study. All other sides are assumed to be thermally insulated. The assumed boundary conditions result into a mode I crack opening problem. The plane strain condition is assumed. The SIF for this two-dimensional thermoelasticity problem is obtained and compared with the analytical solution given by Lee and Sim (1990). This analytical solution is used by Hosseini-Tehrani et al. (2001) to investigate the accuracy of their BEM results. The analytical solution in (Lee and Sim, 1990) is obtained by neglecting the inertia effect so the problem is static in elastic part. The problem dimensions are $h = 2.0$ mm and $w = 1.0$ mm. The crack length is $a = 0.5$ mm. The material properties are $\rho = 7833$ kg/m^3, $E = 200$ GPa, $\nu = 0.30$, $\alpha = 6.68 \times 10^{-6}$ K^{-1}, $c = 461.0$ J/kg K and $k = 17.0$ W/mK. A 60×160 four node rectangular element mesh with 300 time steps is used. The SIF values are plotted versus time in

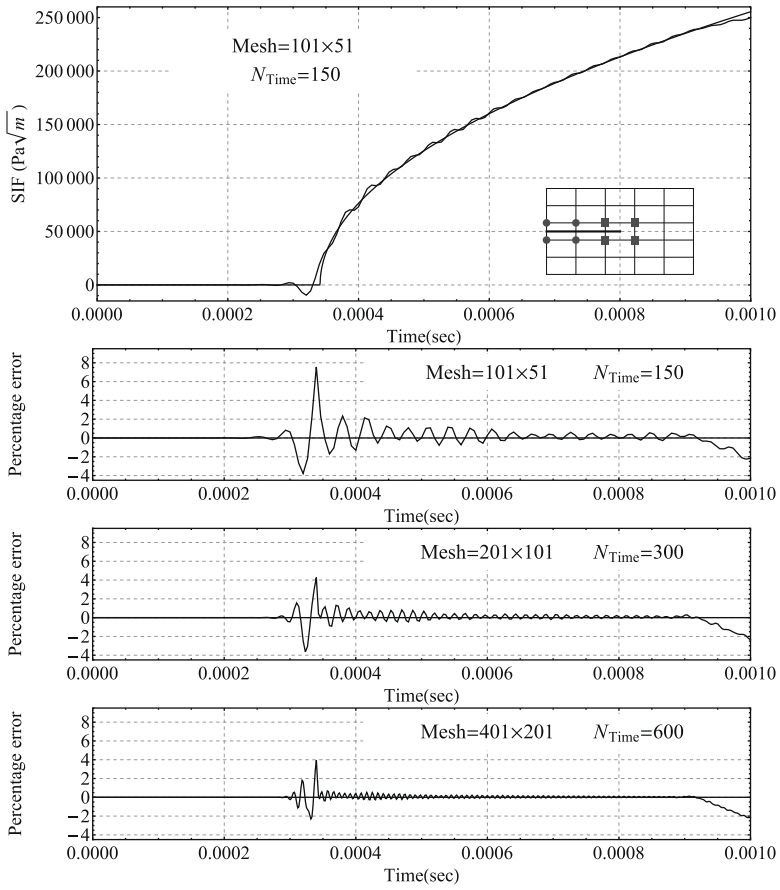

Fig. 8. Stress intensity factor versus time for the case 3 of the first numerical example.

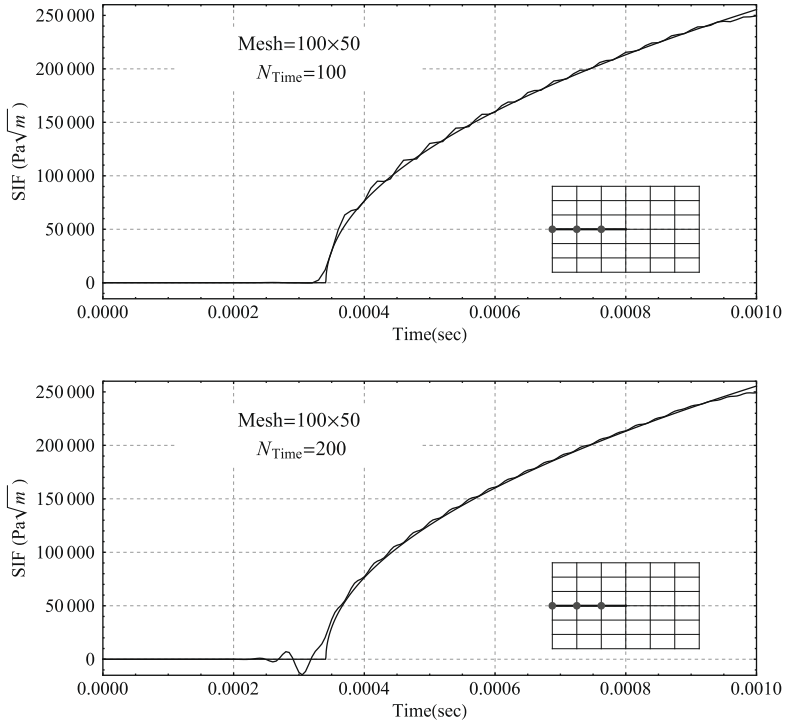

Fig. 9. Stress intensity factor versus time for two different number of time steps for the case 1 of the first numerical example.

Fig. 11. As can be seen form this figure, the numerical results are in good agreement with the analytical values. As mentioned earlier, this problem is defined to be static in elastic part and transient in thermal part to make comparison with the available analytical

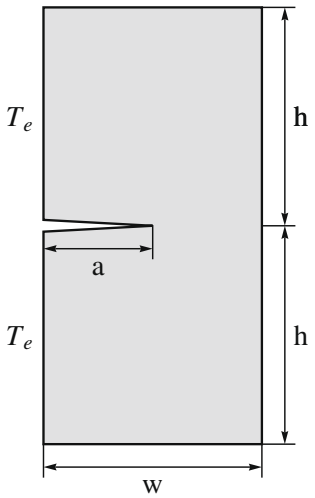

Fig. 10. Second numerical example: edge cracked plate under quasi static thermal shock.

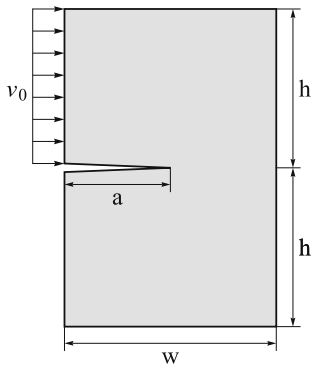

Fig. 12. Third numerical example: edge cracked plate under mixed mode mechanical shock.

solution. The noisy oscillations observed in the first numerical example are absent here. In the region near to the left edge of the cracked body on which the thermal shock is imposed, the temperature variations have some oscillations at the initial times of simulation. But these oscillations do not reach the near crack tip region. The quality of the results before the peak time in Fig. 11 are not quite satisfactory. But it would not be due to the implementation of the XFEM, as the same trend was observed with the use of standard FEM by Zamani and Eslami (2009). The error may be due to the very large gradients at the very initial times of the simulation for which the numerical model is not able to compensate until nearly the peak time.

5.3. Edge cracked plate under mixed mode mechanical shock

An elastic two-dimensional layer with an edge crack is considered, as is shown in Fig. 12. The assumed boundary conditions result into a mixed mode crack problem. The modes I and II stress intensity factors for this two-dimensional elasticity problem are obtained and compared with the analytical solution given by Lee and Freund (1990). This analytical solution is used by Song and Paulino (2006) to investigate the accuracy of their finite element results. The plane strain condition is assumed. As in (Song and Paulino, 2006), a velocity of magnitude $v_0 = 6.5$ m/s is imposed to the upper half of the left edge and no other boundary conditions are prescribed. The layer dimensions are $h = 0.15$ m and $w = 0.1$ m, and the crack length is $a = 0.05$ m. The analytical solution is for an infinite layer so the calculations are stopped at $t = 0.000027$ s before the scattered wave at the crack tip bounces back from the boundary. The material properties are $\rho = 7850$ kg/m^3, $E = 200$ GPa, and $\nu = 0.25$. A 80×150 four node rectangular element mesh with 220 time steps is used.

As can be seen from Fig. 13, there is good agreement between the numerical and analytical SIFs. In this numerical example the mesh resolution is finer than the first mesh resolution used for the case 2 of the first numerical example; but the SIFs are less accurate. In the first numerical example only a dilatation wave with front parallel to the element edges affected the crack tip, but in this numerical example a combination of the dilatation, shear, and the Rayleigh waves propagate through the body. Also, the dilatation waves emanating from the plate corners propagate by a curved front. These would be among the reasons that the SIFs for this numerical example are less accurate compared to the case 2 of the first numerical example.

5.4. Curved crack under dynamic thermal shock

A two-dimensional cracked layer made of Bismuth at $T_0 = 3.5$ K is considered. The layer is exposed to a thermal shock. For Bismuth at low temperature conditions ($T_0 = 3.5$ K), the time scale for the diffusing temperature disturbance is of the same order of the time scale for the propagating displacement wave (Zamani et al., 2009). Thus, in the time interval that temperature varies inside the body, the inertia terms are also excited and the problem should be solved dynamically both in the elastic and thermal parts. As mentioned previously, we have used classical theory of thermoelasticity in

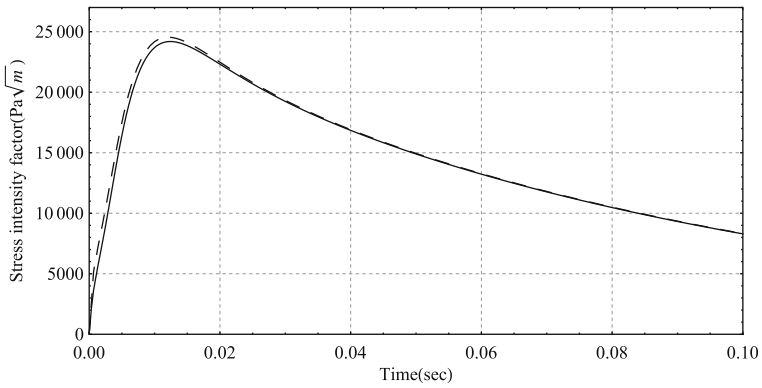

Fig. 11. Stress intensity factor versus time for the second numerical example (dashed line: analytical, solid line: present).

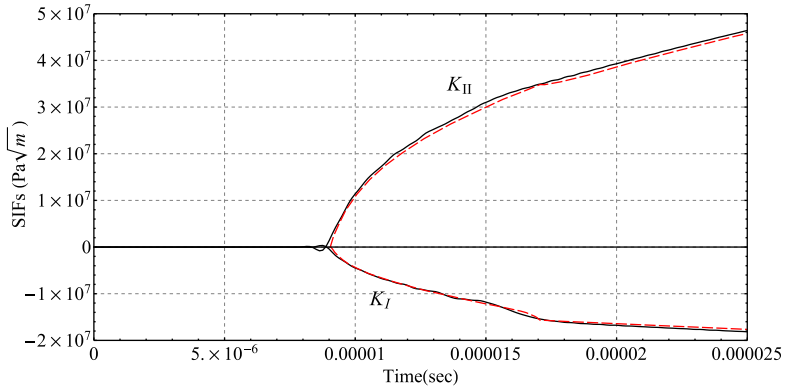

Fig. 13. Stress intensity factor versus time for the third numerical example (dashed line: analytical, solid line: present).

this study. To attain a more realistic model for this numerical example, the generalized theories of thermoelasticity should be used to define wave behaviour for the propagation of thermal disturbances (Hetnarski and Eslami, 2009).

The crack is considered in curved form to invoke the ability of the XFEM in modeling a curved discontinuity independent of the mesh configuration. In the XFEM computer code, the curve is constructed by a collection of straight line segments as proposed in (Sukumar and Prévost, 2003). This would be also a suitable treatment for the case of growing cracks, as in each time step the crack can be assumed to grow one further straight segment. The crack kinks coordinates are given in Table 1 with the coordinate origin located at the left lower corner of the plate in Fig. 14.

The layer is initially at $T_0 = 3.5$ K and then at $t = 0$ a temperature perturbation of $\Delta T = -0.2$ K is applied to the left side (Fig. 14). All other sides are assumed to be thermally insulated. No displacements are defined at the boundaries. The plane strain condition is assumed. The dimensions of the layer are $w = 12.0$ mm, $h_1 = 10.0$ mm and $h_2 = 15.0$ mm. The material properties of Bismuth are considered as: Young's modulus $E = 40.0$ GPa, Poisson's ratio $\nu = 0.3$, density $\rho = 9780.0$ kg/m^3, thermal coefficient $\alpha = 6.75 \times 10^{-6}$ 1/K, specific heat $c = 0.052$ J/kgK and thermal conductivity $k = 875$ W/mK. Two mesh resolutions of 70×141 and 300×605 four node rectangular elements are used in this numerical example. The number of time steps is 90 for the first mesh resolution and 380 for the second one.

The simulation is performed until the time $t = 4.0$ μs. The deformed shape at $t = 3.68$ μs is plotted in Fig. 14. The numerical SIF results for the modes I and II are given in Figs. 15 and 16, respectively. After the thermal shock is applied at the left edge, the stress distribution in the layer is dominated by a dilatation stress wave which moves from left to right in the layer. This stress wave is generated by thermal disturbance which grows in a diffusive manner. Thus, if an observer stands at a point inside the solution domain, at first the stresses increase diffusively to some peak values (negative for σ_{xx} in this example) and then abruptly change sign when the wave front is reached to the observer and

Table 1
Crack kinks coordinates.

Kink number	1	2	3	4	5	6
x (cm)	0.0	0.0833	0.1468	0.2093	0.2700	0.3279
y (cm)	1.0	1.0	1.0038	1.0153	1.0342	1.0603
	7	8	9	10	11	12
x (cm)	0.3823	0.4323	0.4773	0.5165	0.5494	0.5754
y (cm)	1.0932	1.1324	1.1773	1.2273	1.2817	1.3397

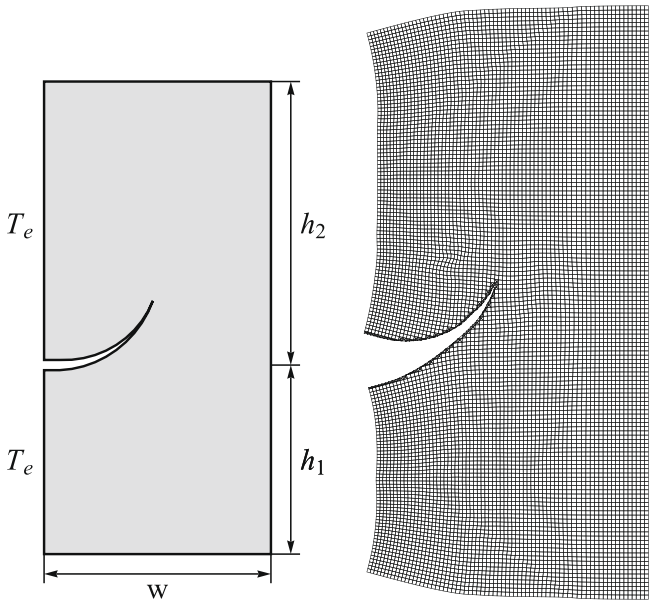

Fig. 14. Fourth numerical example: curved cracked plate under thermal shock (left: geometrical definitions, right: deformed shape at time $t = 3.68$ μs).

then vary smoothly after the wave front is passed. The SIFs variations versus time in Figs. 15 and 16 follow this interpretation for the stress wave variations. The stress wave front reaches the crack tip at $t = 2.45$ μs. As can be seen from Figs. 15 and 16, this corresponds to the peaks for both K_I and K_{II} values versus time. Before that time, the SIF values grow diffusively up to their peak values. After the time $t = 2.45$ μs, the stress wave passes through the crack tip and then abruptly changes sign. Therefore, the SIFs grow in opposite direction and finally their variation becomes smooth by distancing the stress wave front from the crack tip position. The oscillations after the peak time are due to the use of Newmark integration algorithm and spatial discretization in finite element modeling, as it was observed in the previous numerical examples. The values of these unavoidable noisy oscillations depend upon the shape of the displacement wave front which is generally different for the thermal shocks compared to the elastic ones. These oscillations are smaller for the finer mesh resolution as is expected. Due to the presence of the curved crack, there is a very complicated pattern of emanating and reflecting waves traveling in the solution domain. But It seems that the dilatation wave moving from the left edge to the right edge has the major contribution to the SIF variations.

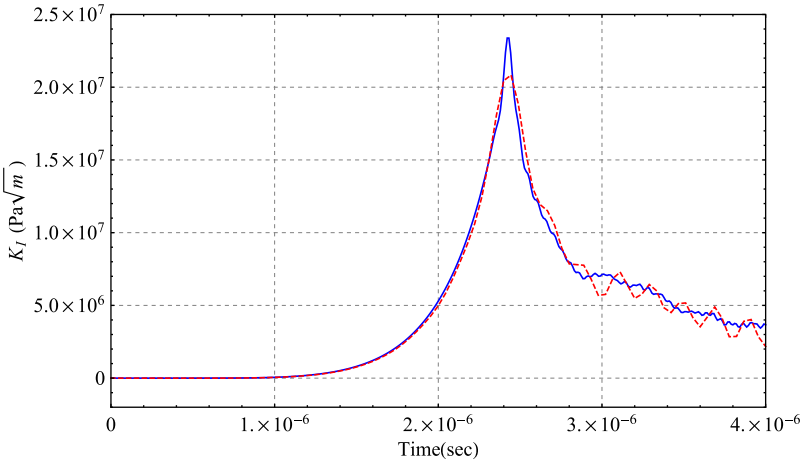

Fig. 15. Mode *I* stress intensity factor versus time for the fourth numerical example (curved crack). The dashed lines are for a mesh of 70 × 141 rectangular elements with $N_{Time} = 90$ time steps and the solid lines are for a mesh of 300 × 605 rectangular elements with $N_{Time} = 380$ time steps.

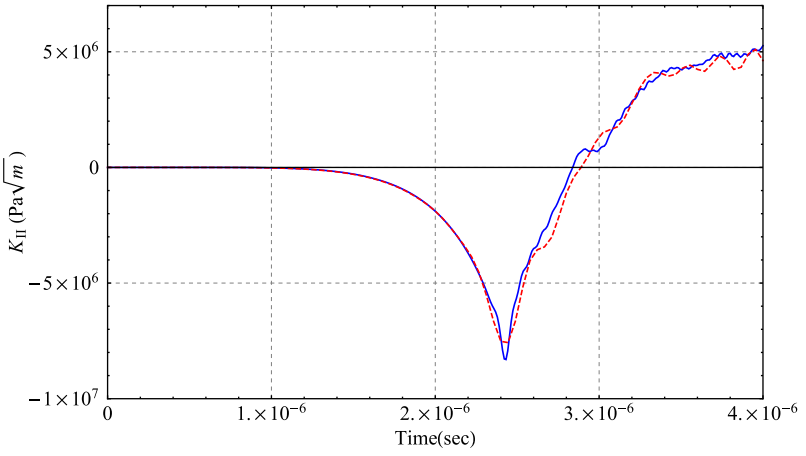

Fig. 16. Mode *II* stress intensity factor versus time for the fourth numerical example (curved crack). The dashed lines are for a mesh of 70 × 141 rectangular elements with $N_{Time} = 90$ time steps and the solid lines are for a mesh of 300 × 605 rectangular elements with $N_{Time} = 380$ time steps.

6. Conclusions

In this study, the XFEM is implemented to model bodies with a stationary crack under dynamic thermo-mechanical loading. Different numerical examples are discussed, including the elastic and thermoelastic problems. The case of a curved crack is also studied in the last numerical example.

While the crack tip enrichment always increases the accuracy of computed SIFs, the error introduced by noisy oscillations, which is inherent in the FEM modeling of wave fronts, weakens the justification for the use of singularity enrichment in the dynamic cases. Another rule of singularity enrichment, which collaborates with discontinuity enrichment to exactly locate the crack tip position, can also be introduced by using a modified version of discontinuity enrichment discussed in (Belytschko et al., 2003). The extensions from original XFEM to space–time XFEM enable the inclusion of discontinuity in both space and time domains (Chessa and Belytschko, 2004; Chessa and Belytschko, 2006; Netuzhylov and Zilian, 2009; Nguyen et al., 2008b). It would be an appealing topic to use the space–time XFEM to suppress the unwanted noisy oscillations in dynamic loading of a cracked body. However the method needs further developments in this direction since until now, it is used only for some simple patterns of discontinuity fronts in the solution domain. There can be a very complicated pattern of emanating and reflecting wave fronts through the body specially for the case of a curved crack. Also, the wave front can have discontinuity in primary variables or discontinuity in derivatives or none of them with only very high gradients that introduce noisy oscillations.

Acknowledgements

The financial support of the National Elite Foundation is gratefully acknowledged.

References

Belytschko, T., Black, T., 1999. Elastic crack growth in finite elements with minimal remeshing. International Journal for Numerical Methods in Engineering 45, 601–620.

Belytschko, T., Chen, H., Xu, J., Zi, G., 2003. Dynamic crack propagation based on loss of hyperbolicity and a new discontinuous enrichment. International Journal for Numerical Methods in Engineering 58, 1873–1905.

Bordas, S., Duflot, M., 2007. Derivative recovery and a posteriori error estimate for extended finite elements. Computer Methods in Applied Mechanics and Engineering 196, 3381–3399.

Bordas, S., Nguyen, P.V., Dunant, C., Guidoum, A., Nguyen-Dang, H., 2007. An extended finite element library. International Journal for Numerical Methods in Engineering 71, 703–732.
Bordas, S.P.A., Rabczuk, T., Hung, N.-X., Nguyen, V.P., Natarajan, S., Bog, T., Quan, D.M., Hiep, N.V., 2009. Strain smoothing in FEM and XFEM. Computers and Structures. Doi: 10.1016/j.compstruc.2008.07.006.
Chessa, J., Belytschko, T., 2004. Arbitrary discontinuities in space time finite elements by level sets and X-FEM. International Journal for Numerical Methods in Engineering 61, 2595–2614.
Chessa, J., Belytschko, T., 2006. A local space time discontinuous finite element method. Computer Methods in Applied Mechanics and Engineering 195, 1325–1343.
Chessa, J., Smolinski, P., Belytschko, T., 2002. The extended finite element method (X-FEM) for solidification problems. International Journal for Numerical Methods in Engineering 53 (7), 1957–1977.
Daux, C., Moës, N., Dolbow, J., Sukumar, N., Belytschko, T., 2000. Arbitrary branched and intersecting cracks with the extended finite element method. International Journal for Numerical Methods in Engineering 48, 1741–1760.
Dell'Erba, D.N., Aliabadi, M.H., Rooke, D.P., 1998. Dual boundary element method for three-dimensional thermoelastic crack problems. International Journal of Fracture 94, 89–101.
Dolbow, J., Moës, N., Belytschko, T., 2000. Discontinuous enrichment in finite elements with a partition of unity method. Finite Elements in Analysis and Design 36, 235–260.
Dongarra, J., Lumsdaine, A., Pozo, R., Remington, K., 1998. IML++ version 1.2: Iterative methods library reference guide. National Institute of Standards and Technology, University of Notre Dame, Available from: %3chttp://math.nist.gov/iml++%3e.
Duarte, C.A., Hamzeh, O.N., Liszka, T.J., Tworzydlo, W.W., 2001. A generalized finite element method for the simulation of three dimensional dynamic crack propagation. Computer Methods in Applied Mechanics and Engineering 190, 2227–2262.
Duddu, R., Bordas, S., Chopp, D., Moran, B., 2008. A combined extended finite element and level set method for biofilm growth. International Journal for Numerical Methods in Engineering 74, 848–870.
Duddu, R., Chopp, D.L., Moran, B., 2009. A two-dimensional continuum model of biofilm growth incorporating fluid flow and shear stress based detachment. Biotechnology and Bioengineering 103, 92–104.
Duflot, M., 2008. The extended finite element method in thermoelastic fracture mechanics. International Journal for Numerical Methods in Engineering 74, 827–847.
Duflot, M., Bordas, S., 2008. A posteriori error estimation for extended finite elements by an extended global recovery. International Journal for Numerical Methods in Engineering 76, 1123–1138.
Dumstorff, P., Meschke, G., 2007. Crack propagation criteria in the framework of X-FEM-based structural analyses. International Journal for Numerical and Analytical Methods in Geomechanics 31, 239–259.
Elguedj, T., Gravouil, A., Combescure, A., 2007. A mixed augmented Lagrangian-extended finite element method for modelling elastic plastic fatigue crack growth with unilateral contact. International Journal for Numerical Methods in Engineering 71, 1569–1597.
Eslami, M.R., 2003. A First Course in Finite Element Analysis. Tehran Publication Press.
Freund, L.B., 1990. Dynamic Fracture Mechanics. Cambridge University Press, Cambridge.
Fries, T.-P., 2008. A corrected XFEM approximation without problems in blending elements. International Journal for Numerical Methods in Engineering 75, 503–532.
Gracie, R., Ventura, G., Belytschko, T., 2007. A new fast method for dislocations based on interior discontinuities. International Journal for Numerical Methods in Engineering 69, 423–441.
Gravouil, A., Moës, N., Belytschko, T., 2002. Non-planar 3d crack growth by the extended finite element and level sets, part II: level set update. International Journal for Numerical Methods in Engineering 53 (11), 2569–2586.
Hetnarski, R.B., Eslami, M.R., 2009. Thermal Stresses – Advanced Theory and Applications. Solid Mechanics and Its Applications, vol. 158. Springer.
Hosseini-Tehrani, P., Eslami, M.R., Azari, S.H., 2006. Analysis of thermoelastic crack problems using Green–Lindsay theory. Journal of Thermal Stresses 29, 317–330.
Hosseini-Tehrani, P., Eslami, M.R., Daghyani, H.R., 2001. Dynamic crack analysis under coupled thermoelastic assumption. Journal of Applied Mechanics 68 (4), 584–588.
Hughes, T.J.R., Belytschko, T., 2000. Nonlinear Finite Element Analysis. ICE Division, Zace Services Ltd..
Huynh, D.B.P., Belytschko, T., 2009. The extended finite element method for fracture in composite materials. International Journal for Numerical Methods in Engineering 77, 214–239.
Laborde, P., Pommier, J., Renard, Y., Salaün, M., 2005. High-order extended finite element method for cracked domains. International Journal for Numerical Methods in Engineering 64, 354–381.
Lee, K.Y., Sim, K.B., 1990. Thermal shock stress intensity factor by Bueckner's weight function method. Engineering Fracture Mechanics 37 (4), 799–804.
Lee, Y.J., Freund, L.B., 1990. Fracture initiation due to asymmetric impact loading of an edge cracked plate. Journal of Applied Mechanics 57, 104–111.
Legay, A., Chessa, J., Belytschko, T., 2006. An Eulerian–Lagrangian method for fluid–structure interaction based on level sets. Computer Methods in Applied Mechanics and Engineering 195 (17–18), 2070–2087.
Liu, G., Dai, K., Nguyen, T., 2006. A smoothed finite element for mechanics problems. Computational Mechanics 39, 859–877.
Melenk, J.M., Babuska, I., 1996. The partition of unity finite element method: basic theory and applications. Computer Methods in Applied Mechanics and Engineering 139, 289–314.
Moës, N., Belytschko, T., 2002. Extended finite element method for cohesive crack growth. Engineering Fracture Mechanics 69 (2), 813–833.
Moës, N., Dolbow, J., Belytschko, T., 1999. A finite element method for crack growth without remeshing. International Journal for Numerical Methods in Engineering 46, 131–150.
Moës, N., Gravouil, A., Belytschko, T., 2002. Non-planar 3d crack growth by the extended finite element and level sets, part I: mechanical model. International Journal for Numerical Methods in Engineering 53 (11), 2549–2568.
Mousavi, S.E., Xiao, H., Sukumar, N., 2009. Generalized gaussian quadrature rules on arbitrary polygons. International Journal for Numerical Methods in Engineering. Doi: 10.1002/nme.2759.
Natarajan, S., Bordas, S., Mahapatra, D.R., 2009. Numerical integration over arbitrary polygonal domains based on Schwarz–Christoffel conformal mapping. International Journal for Numerical Methods in Engineering 80, 103–134.
Netuzhylov, H., Zilian, A., 2009. Space–time meshfree collocation method: methodology and application to initial-boundary value problems. International Journal for Numerical Methods in Engineering 80, 355–380.
Newmark, N.M., 1959. A method of computation for structural dynamics. Journal of Engineering Mechanics Division, ASCE 85, 67–94.
Nguyen, N.T., Rabczuk, T., NguyenXuan, H., Bordas, S., 2008a. A smoothed finite element method for shell analysis. Computer Methods in Applied Mechanics and Engineering 198, 165–177.
Nguyen, V.P., Rabczuk, T., Bordas, S., Duflot, M., 2008b. Meshless methods: a review and computer implementation aspects. Mathematics and Computers in Simulation 79, 763–813.
Nguyen-Xuan, H., Rabczuk, T., Bordas, S., Debongnie, J.F., 2008. A smoothed finite element method for plate analysis. Computer Methods in Applied Mechanics and Engineering 197, 1184–1203.
Pozo, R., Remington, K., Lumsdaine, A., 1998. SparseLib++ version 1.7: Sparse Matrix Library. National Institute of Standards and Technology, University of Notre Dame, Available fromt %3chttp://math.nist.gov/sparselib++%3e.
Prasad, N.N.V., Aliabadi, M.H., Rooke, D.P., 1994. The dual boundary element method for thermoelastic crack problems. International Journal of Fracture 66, 255–272.
Prasad, N.N.V., Aliabadi, M.H., Rooke, D.P., 1996. The dual boundary element method for transient thermoelastic crack problems. International Journal of Solids and Structures 33, 2695–2718.
Raveendra, S.T., Banerjee, P.K., 1992. Boundary element analysis of cracks in thermally stressed planar structures. International Journal of Solids and Structures 29, 2301–2317.
Réthoré, J., Gravouil, A., Combescure, A., 2004. A stable numerical scheme for the finite element simulation of dynamic crack propagation with remeshing. Computer Methods in Applied Mechanics and Engineering 193, 4493–4510.
Réthoré, J., Gravouil, A., Combescure, A., 2005. An energy-conserving scheme for dynamic crack growth using extended finite element method. International Journal for Numerical Methods in Engineering 63, 631–659.
Shih, C.F., Moran, B., Nakamura, T., 1986. Energy release rate along a three-dimensional crack front in a thermally stressed body. International Journal of Fracture 30, 79–102.
Sih, G.C., 1962. On singular character of thermal stress near a crack tip. Journal of Applied Mechanics 51, 587–591.
Song, J.-H., Belytschko, T., 2009. Cracking node method for dynamic fracture with finite elements. International Journal for Numerical Methods in Engineering 77, 360–385.
Song, S.H., Paulino, G.H., 2006. Dynamic stress intensity factors for homogeneous and smoothly heterogeneous materials using the interaction integral method. International Journal of Solids and Structures 43, 4830–4866.
Sukumar, N., 2000. Element partitioning code in 2-d and 3-d for the extended finite element method. Available from: %3chttp://dilbert.engr.ucdavis.edu/suku/xfem%3e.
Sukumar, N., Huang, Z.Y., Prévost, J.-H., Suo, Z., 2003a. Partition of unity enrichment for bimaterial interface cracks. International Journal for Numerical Methods in Engineering 59 (8), 1075–1102.
Sukumar, N., Moës, N., Moran, B., Belytschko, T., 2000. Extended finite element method for three dimensional crack modeling. International Journal for Numerical Methods in Engineering 48, 1549–1570.
Sukumar, N., Prévost, J.-H., 2003. Modeling quasi-static crack growth with the extended finite element method, part I: computer implementation. International Journal of Solids and Structures 40, 7513–7537.
Sukumar, N., Srolovitz, D.J., Baker, T.J., Prevost, J.-H., 2003b. Brittle fracture in polycrystalline microstructures with the extended finite element method. International Journal for Numerical Methods in Engineering 56 (14), 2015–2037.
Ventura, G., 2006. On the elimination of quadrature subcells for discontinuous functions in the extended finite element method. International Journal for Numerical Methods in Engineering 66, 761–795.
Ventura, G., Gracie, R., Belytschko, T., 2009. Fast integration and weight function blending in the extended finite element method. International Journal for Numerical Methods in Engineering 77, 1–29.

Ventura, G., Moran, B., Belytschko, T., 2005. Dislocations by partition of unity. International Journal for Numerical Methods in Engineering 62, 1463–1487.
Wilson, W.K., Yu, I.W., 1979. The use of the *J*-integral in thermal stress crack problems. International Journal of Fracture 15, 377–387.
Zamani, A., Eslami, M.R., 2009. Coupled dynamical thermoelasticity of a functionally graded cracked layer. Journal of Thermal Stresses 32, 969–985.
Zamani, A., Hetnarski, R.B., Eslami, M.R., 2009. Second sound in a cracked layer based on lord-shulman theory. In: Thermal Stresses Congress, Illinois, USA.
Zi, G., Belytschko, T., 2003. New crack-tip elements for XFEM and applications to cohesive cracks. International Journal for Numerical Methods in Engineering 57, 2221–2240.